EXPERIMENTAL STUDY OF TSUNAMI-INDUCED FORCES ON ONSHORE SEAWALLS

by

Naoki Furuichi[1], Y. Ohmura[2], H. Yagi[3], A. Nakayama[4], M. Yoneyama[5], H. Kato[6], and A. Kado[7]

ABSTRACT

Several "onshore" seawalls, built behind the fishing ports to protect villages, collapsed because of the tsunami that immediately followed the Great East Japan Earthquake on March 11, 2011. As seawalls collapsed frequently regardless of the scouring due to tsunami overflow, we reconsidered the methods of calculating tsunami-induced hydrodynamic forces. In this study, we conducted hydraulic model experiments to evaluate tsunami-induced forces acting on onshore seawalls under non-overflow and overflow conditions. On the basis of the obtained results, we proposed formulae to calculate the tsunami-induced forces under the non-overflow condition using 1) the hydrostatic pressure relation and a correction factor of 1.1, and 2) using a quadratic function of the Froude number. Under the overflow condition, we proposed a calculation formula using the inundation depths in front of and behind the seawalls.

1. INTRODUCTION

The Great East Japan Earthquake (magnitude 9.0) and the resulting tsunami on March 11, 2011 caused serious damage to the fishing ports and villages of Japan. It is believed that the external forces that acted on the fishing port facilities far surpassed the conventional design requirements.

Field surveys, conducted after the earthquake, reported that several "onshore" seawalls, built behind the fishing ports to protect the villages, collapsed because of the tsunami (**Figures 1 and 2** show the examples of disaster areas and seawalls). Although the major reason for the collapse was scouring due to tsunami overflow, seawalls collapsing without any scouring were also frequently reported. On the other hand, in the conventional design methods, tsunami-induced forces are often calculated based on the hydrostatic pressure profile corresponding to the inundation depth of a tsunami (e.g., Japan Society of Civil Engineers 2004). In other words, partly because the period of a tsunami is significantly greater than that of wind waves, the conventional methods only considered the water level effect, but seldom considered the effect of dynamic pressure (movement of water).

Although recent studies have examined the wave forces acting on breakwaters, onshore structures, and bridge superstructures (Tanimoto et al. 1984, Asakura et al. 2000, 2002, Nakamura et al. 2016) and the characteristics of tsunami's inundation after the earthquake (Adriano et al. 2016), the effects of the slope of the bottom topography, the slope of the seawall structure, and the distance of the structure from the shoreline were not fully understood. Furthermore, few studies have investigated the wave-force characteristics of onshore structures under tsunami overflow conditions; in particular, the characteristics of wave forces acting on the landward side of a seawall are poorly understood. Hence, we modified the methods of calculating the tsunami-induced forces acting on seawalls.

1 National Research Institute of Fisheries Engineering, Japan Fisheries Research and Education Agency, Japan, furu1naoki@affrc.go.jp

2 National Research Institute of Fisheries Engineering, Japan Fisheries Research and Education Agency, Japan

3 National Defense Academy, Japan

4 National Research Institute of Fisheries Engineering, Japan Fisheries Research and Education Agency, Japan. Currently, Alpha Hydraulic Engineering Consultants, Co. LTD, Japan

5 Reconstruction Agency, Japan

6 The Japanese Institute of Fisheries Infrastructure and Communities, Japan

7 International Meteorological & Oceanographic Consultants Co. Ltd., Japan
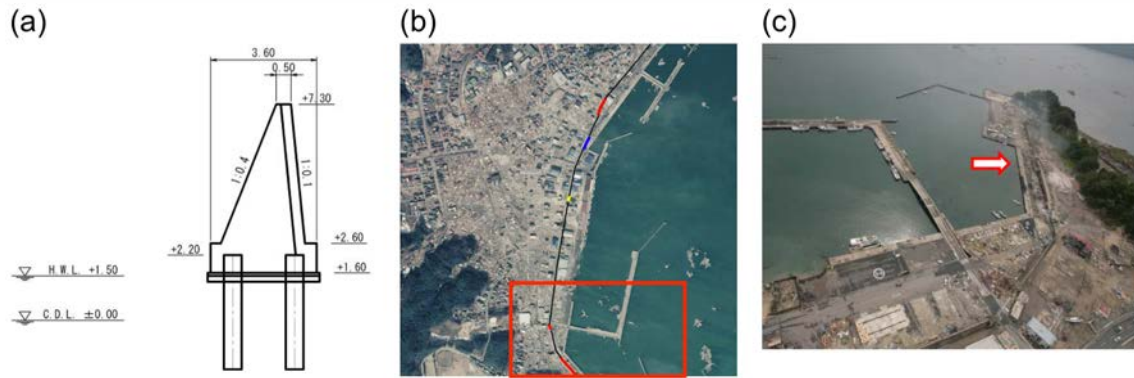
Figure 1: (a) A cross-sectional view of tsunami-affected seawall, (b) Example of seawall position (black-colored line). The red-colored line indicates the position of tsunami-affected seawall whose construction is similar to (a), and (c) Aerial photograph of the red-colored box area in (b). The arrow indicates a tsunami-affected area. (From the website of National Research Institute of Fisheries Engineering, Japan)

Figure 2: Images of tsunami-affected seawalls confirmed in the red-colored box area in Figure 1(b). (From the website of National Research Institute of Fisheries Engineering, Japan)

Recently, we conducted hydraulic model experiments to evaluate the tsunami-induced forces acting on onshore seawalls by changing the conditions of the slope of the bottom topography, the slope of the seawall structure, and the distance of the seawall from the shoreline (Ohmura et al. 2014, 2015). Based on the results obtained, we explored the methods of calculating the wave forces under non-overflow and overflow conditions with special attention on comparing the measured wave pressure to that predicted using the hydrostatic pressure relation. In this paper, we introduce the main results of the previous papers.
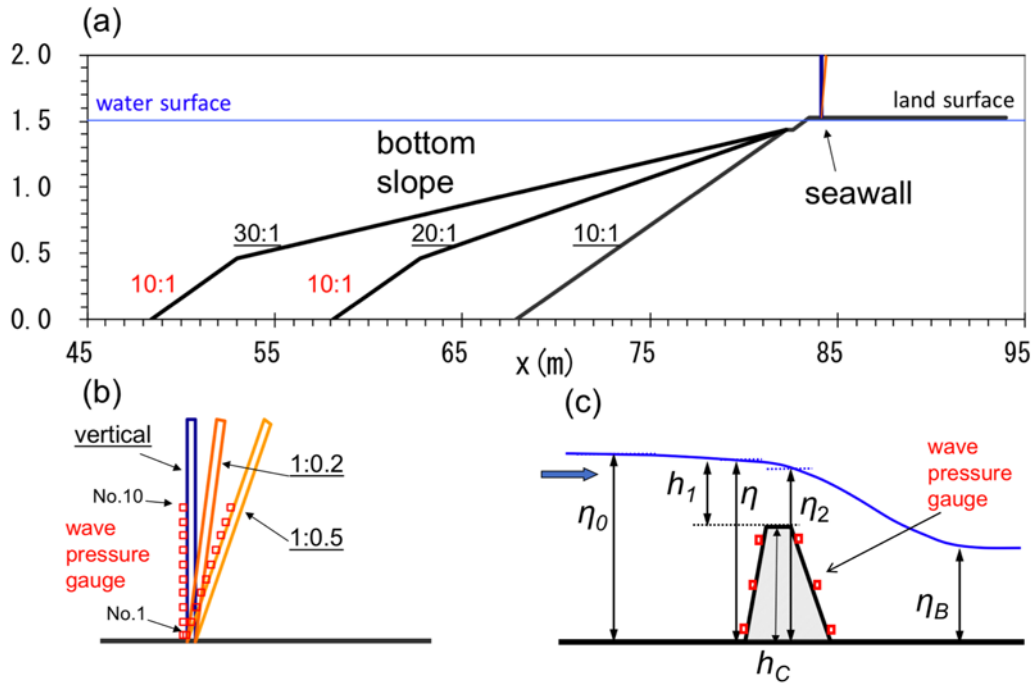
Figure 3: (a) Sketch of wave flume layout, (b) Position of wave pressure gauge for the non-overflow cases, and (c) Position of wave pressure gauge for the overflow cases.

2. HYDRAULIC MODEL EXPERIMENTS

Figure 3 and Tables 1 and 2 summarize the overview of the present experiment. The experiments were performed in a wave flume (100 m in length, 2 m in height, and 1 m in width) on a scale of 1/81. Beginning at the wavemaker, the bathymetry consisted of a 47–68 m flat-ocean bottom section, a 17–38 m slope section, and a 15-m flat-land surface section. We installed three types of bottom slopes with ratios of 30:1, 20:1, and 10:1. The seawall was positioned at the point where the distance from the shoreline (x) is in the range of 0–150 m (unless otherwise stated, the experimental parameters mentioned herein are described according to the corresponding local scale). The seawall height was set such that it satisfactorily exceeded the tsunami inundation depth for the non-overflow conditions (**Figure 3(b)**). Moreover, it was set in the range of 4.6–8.3 m for the overflow conditions (**Figure 3(c)**). The shoreward slopes of the seawall were set to 1:0 (vertical), 1:0.2, and 1:0.5, whereas the landward slope was set to 1:0.5.

(a) Non-overflow condition			(b) Overflow condition			
Bottom slope	Distance from shoreline (local scale)	Shoreward slope of seawall	Bottom slope	Distance from shoreline (local scale)	Seawall height (local scale)	Shoreward slope of seawall
(s_B)	(x)	(s_W)	(s_B)	(x)	(h_C)	(s_W)
30:1 20:1 10:1	0 m 25 m 50 m 75 m 100 m 150 m	vertical (1:0) 1:0.2 1:0.5	30:1 20:1 10:1	0 m 50 m 100 m	4.6 m 6.4 m 8.3 m	vertical (1:0) 1:0.2 1:0.5

Table 1: Experimental conditions of present study. The values for the distance from the shore line (x) and the seawall height (h_c) are described according to the corresponding local scale.

3

No.	Offshore wave height	Wave period ($T/2$)
1	8.1 cm (6.6 m)	12.5 s (half period 113 s)
2	6.7 cm (5.4 m)	15.0 s (half period 135 s)
3	5.0 cm (4.1 m)	20.0 s (half period 180 s)

Table 2: Experimental parameters of incident waves. The values based on the corresponding local scale are shown in brackets.

Using forward paddle movement, the tsunami was modeled as an idealized solitary wave with half-periods of 113, 135, and 180 s, corresponding to offshore wave heights of 6.6, 5.4, and 4.1 m, respectively (**Table 2**). In addition, we performed experiments considering the tsunami inundation without the seawall model. The local free surface elevation was measured using wave height gauges with a sampling interval of 50 Hz at locations including the offshore of the shoreline, mid-point between the shoreline and the seawalls, and just in front of the seawall for non-overflow cases. For the overflow cases, the height behind the seawalls was also measured (e.g., η_B in **Figure 3(c)**). The pressure was measured using 6 to 10 wave pressure gauges with a sampling interval of 1000 Hz at different locations on the seawalls (**Figures 3(b) and (c)**). For the wave pressure, we used 10-Hz moving averaged data in later analyses.

3. RESULTS AND DISCUSSIONS

3.1   Overview of freely propagating tsunami flow

Prior to discussing the wave pressure acting on the seawalls, we first examined the characteristics of freely propagating tsunami flow (e.g., see the dashed line in **Figure 4(a)**) reproduced by conducting non-seawall experiments. **Figures 5(a) and (b)** show the distributions of the maximum inundation depth of the freely propagating tsunami (η_{max}) at each point and of the near-bed horizontal velocity (U) measured 0.01 m above the land surface (laboratory scale) when η_{max} was measured.

Figure 5(a) shows that the inundation depth (η_{max}) reached up to ~8.1 m at shoreline ($x = 0$). Along with an increase in the distance from the shoreline (x), a decrease in η_{max} and an increase in U were confirmed. Consequently, the Froude number (Fr) calculated using

$$Fr = \frac{U}{\sqrt{g\eta_{max}}} \tag{1}$$

(where g is the acceleration due to gravity) also increased with the increase in the distance from the shoreline (**Figure 5(c)**). Note that the horizontal axis in Figure 5(c) indicates the ratio of x to the offshore wave length (L), which is determined as follows.

$$L = \sqrt{gh} \times T \tag{2}$$
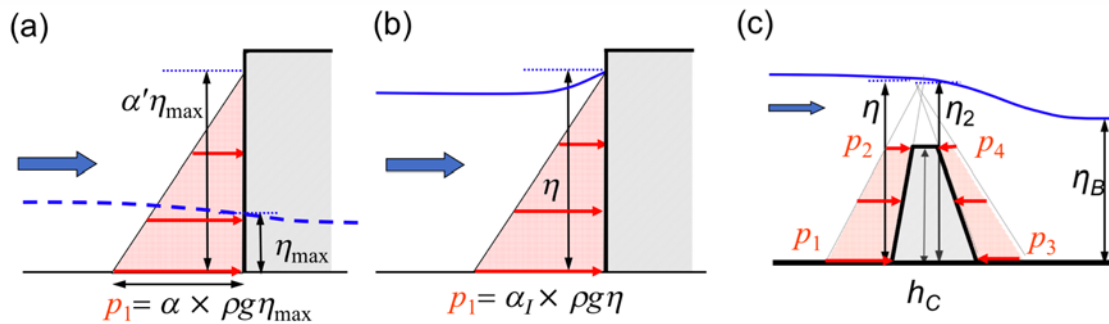
Figure 4: (a) Schematic view of tsunami-induced forces under non-overflow conditions where η_{max} is referred, (b) non-overflow conditions where η is referred, and (c) overflow conditions. The present study assumed that the wave pressure increases linearly in the downward direction.
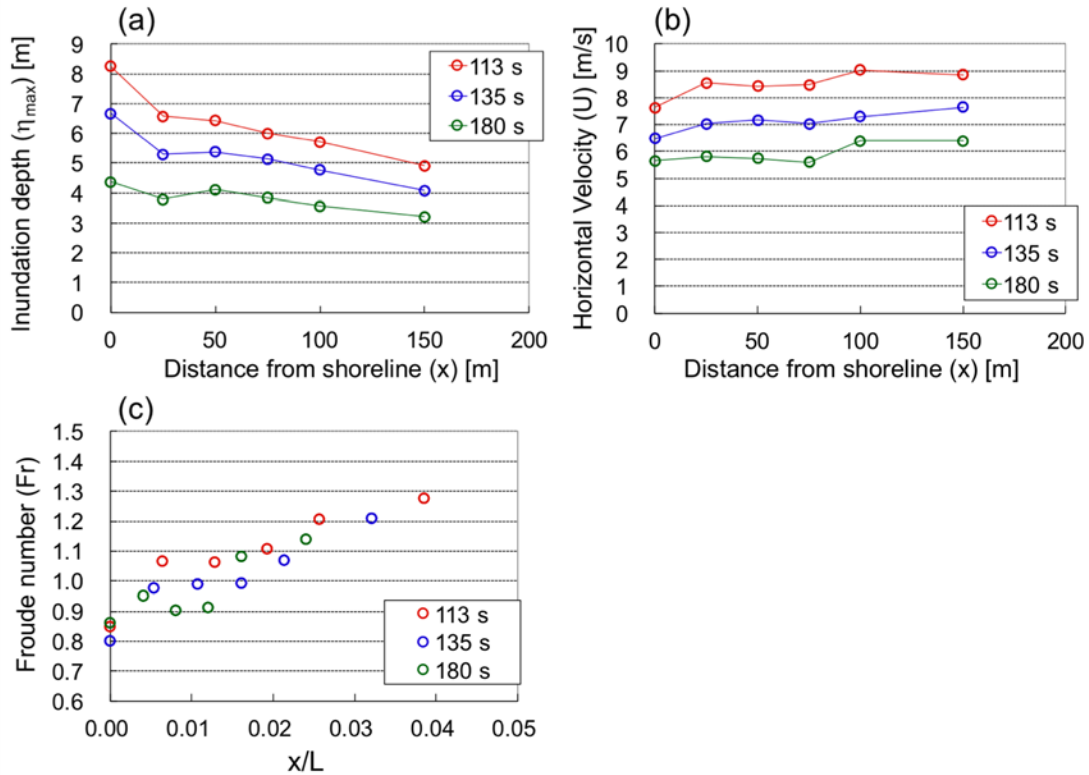
Figure 5: (a) Distribution of η_{max}, (b) horizontal velocity (U), and (c) corresponding Froude number (Fr). The red, blue, and green colors denote wave periods of 113 s, 135 s, and 180 s, respectively.

where h (= ~121 m; local scale) is the offshore water depth. The ranges of x/L and Fr in the present experiment were $0 < x/L < 0.04$ and $0.8 < Fr < 1.3$, respectively.

3.2   Non-overflow cases

3.2.1   Results

Figure 6 shows a laboratory image for the non-overflow cases as well as the time series of the wave pressure and inundation depth in front of the seawall (η, see **Figure 4(b)**). As indicated by the red arrow
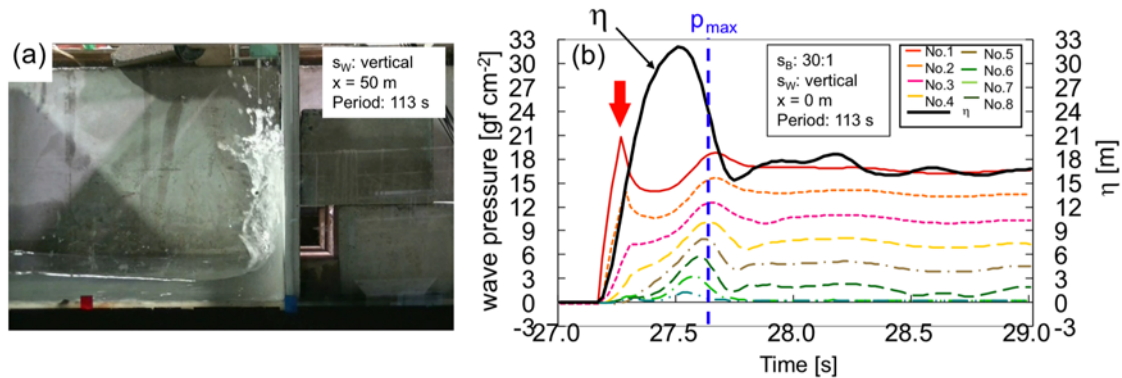
Figure 6: (a) Laboratory image of non-overflow tsunami action, and (b) Sample time series of wave pressure and inundation depth (η). The vertical blue line indicates the time when p_{max} is measured.
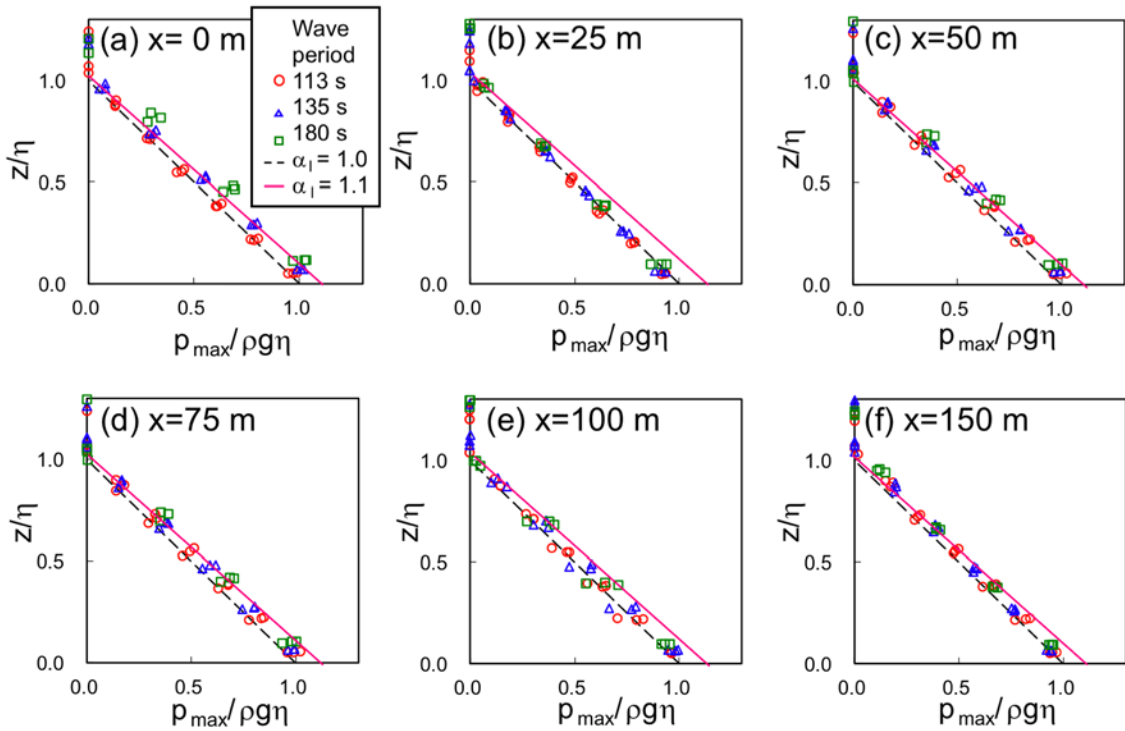
Figure 7: Comparison of vertical profiles of $p_{max}/\rho g\eta$ (symbols) classified in terms of the distance from the shoreline (x) (a to f) and the wave period (red, blue, and green symbols); and those of the corresponding hydrostatic pressure ($p_{max} = \alpha \times \rho g\eta$). The red and black lines represent $\alpha = 1.1$ and $\alpha = 1.0$, respectively.

in **Figure 6(b)**, a local maximum of the wave pressure is confirmed in the case with a wave period of 113 s before η becomes maximum (black line in **Figure 6(b)**). On the other hand, the maximum vertically integrated wave pressure (i.e., the wave force) is measured after η becomes maximum (vertical blue line). In this study, we analyzed the experimental results by focusing on the vertical profiles of the "maximum" wave pressure (p_{max}) when the corresponding wave force was maximum.

Figures 7 and 8 show the vertical profiles of the normalized wave pressure $p_{max}/\rho g\eta$ (where ρ is the density of water, and η is the value when p_{max} was measured). We found that $p_{max}/\rho g\eta$ was not

(x = 50 m; wave period 113-180 s)
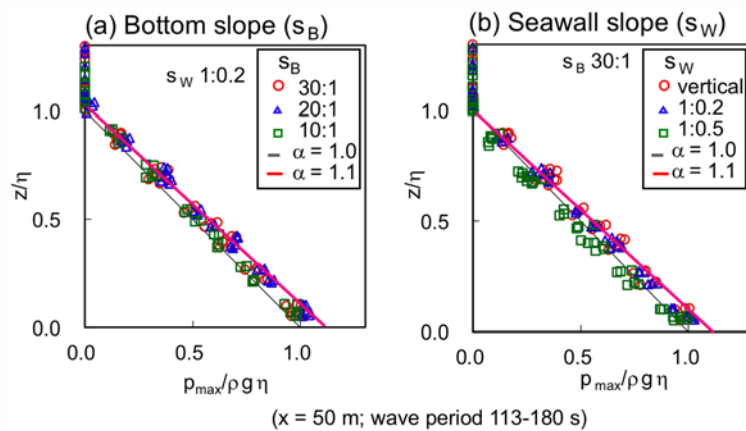
Figure 8: Comparison of vertical profiles of $p_{max}/\rho g\eta$ (symbols) classified in terms of (a) bottom slope s_B, and (b) s_W; and those of the corresponding hydrostatic pressure ($p_{max} = \alpha \times \rho g\eta$) (lines). The red and black lines represent $\alpha = 1.1$ and $\alpha = 1.0$, respectively.
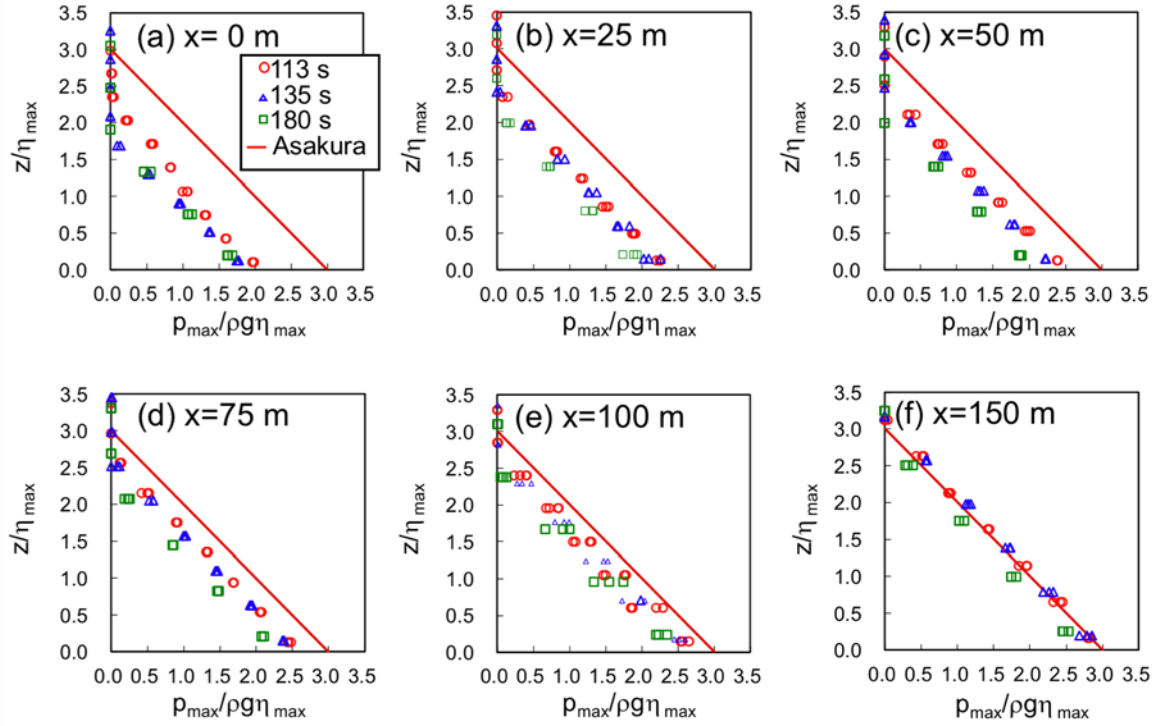
Figure 9: Comparison of vertical profiles of $p_{max}/\rho g\eta_{max}$ (red, blue, and green symbols) and those predicted by Asakura et al. (2000) (red line) classified in terms of the distance from the shoreline (x).

remarkably affected by the change in the slope of the bottom topography (s_B), the slope of the seawall (s_W), the period of the incident wave (T), or the distance of the seawall from the shoreline (x). Moreover, the value of $p_{max}/\rho g\eta$ increased roughly linearly in the downward direction, along with the red and black lines indicating the hydrostatic pressure relation. The ratio of $p_{max}/\rho g\eta$ to the normalized hydrostatic pressure z/η (where z is the height from the land surface) was largely in the range of 1.0–1.1.

As previous studies investigated the wave-force characteristics using η_{max}, (Tanimoto 1984, Asakura et al. 2000), we examined the vertical profile of $p_{max}/\rho g\eta_{max}$ (**Figure 9**), where η_{max} is the value when p_{max} was measured. The figure shows that $p_{max}/\rho g\eta_{max}$ increases with an increase in the distance from the shoreline (x), reaching the values proposed by Asakura et al. (2000) (red line in **Figure 9**).

$$p_{max} = \rho g\left(3 \times \eta_{max} - z\right) \tag{3}$$

As shown in **Figures 9(a)–(f)** and **Figures 10(a) and (b)**, the values of $p_{max}/\rho g\eta_{max}$ are not significantly affected by the changes in the wave period, bottom slope, or seawall slope. As indicated by previous studies on onshore structures (e.g., Afmad et al. 2009) and from **Figure 5(b)**, it is believed that the increase in p_{max} with the increase in the distance from the shoreline (x) is due to the change in the Froude number (Fr).

To evaluate the relationship between Fr and increase in p_{max}, we introduced a correction factor (α_{E1}) defined as follows.

$$\alpha_{E1} = 1 + \overline{\frac{p_{max}}{\rho g\eta_{max}} - \left(1 - \frac{z}{\eta_{max}}\right)} \tag{4}$$

where the overbar denotes the arithmetic mean for heights (z) < ~ 15 m (local scale) in each vertical profile, and the second term in the right-hand side indicates the difference in the measured normalized pressure at each point from the value predicted using the hydrostatic pressure relation.

Figure 10(c) shows the comparisons of Fr and α_{E1} for the non-overflow cases. Although the present results roughly agree with the linear relation proposed by Sakakiyama (2012) (blue line in **Figure 10(c)**), i.e.,
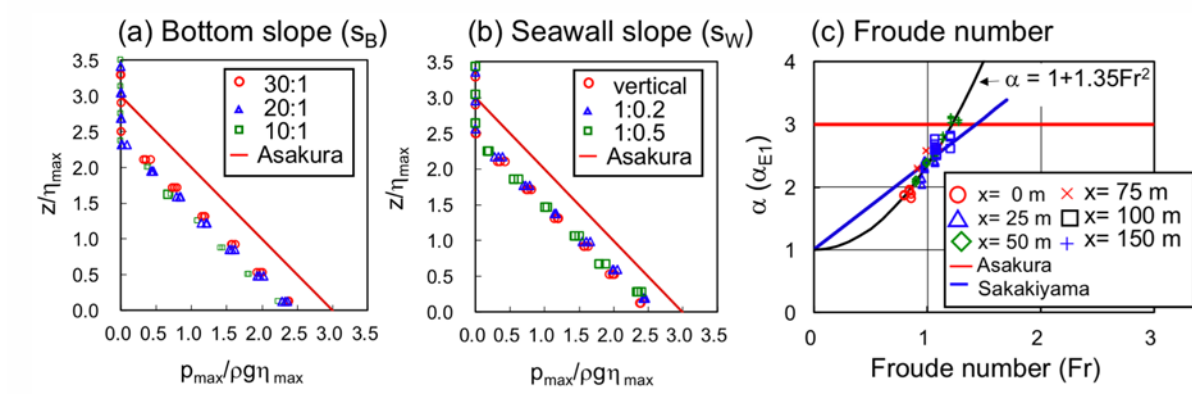
Figure 10: (a, b) Comparison of vertical profiles of $p_{max}/\rho g \eta_{max}$ classified in terms of (a) bottom slope (s_B), (b) seawall slope (s_w), and (c) Ratio of $p_{max}/\rho g \eta_{max}$ to z/η_{max} (α) as a function of the Froude number (Fr). The brown and blue lines indicate those predicted by Asakura et al. (2000) and Sakakiyama (2012), respectively.

$$\alpha = 1 + 1.4Fr, \tag{5}$$

we found that the results agree better with a quadratic relation (cf. Matsutomi et al. 2013) (black line in **Figure 10(c)**), i.e.,

$$\alpha = 1 + 1.35Fr^2 \tag{6}$$

in terms of the root-mean-square error.

3.2.2 Proposed formula

On the basis of the results obtained, we proposed formulae to calculate the tsunami-induced forces under the non-overflow condition to be used in the facility design, as shown below.

First, when the inundation depth in front of the seawall (η) is known, the pressure near the land surface (p_1, **Figure 4(b)**) can be calculated as follows.

$$p_1 = \alpha_I \times \rho g \eta, \ \alpha_I = 1.1 \tag{7}$$

It should be noted that we assumed that the wave pressure increases linearly in the downward direction. Furthermore, when the inundation depth of the freely propagating tsunami (η_{max}) and the corresponding Froude number (Fr) are known, the pressure (p_1) and the operative inundation depth ($\alpha'\eta_{max}$) (**Figure 4(a)**) can be calculated as follows.

$$p_1 = \alpha \times \rho g \eta_{max}, \ \alpha' = \max(3, \alpha) \tag{8}$$

where α can be determined using (6). Note that we proposed the value of α' as the value that is greater between 3 and α in order to evaluate it as a safe-side value. It should also be noted that the present experiment covered only for $0.8 < Fr < 1.3$ (**Figure 5(c)**). However, considering the fact that Sakakiyama (2012) confirmed the available range of the proposed relation (4) for $0 < Fr < 2$, we assumed that (8) can be used when $0 < Fr < 1.5$. If Fr is unknown, the pressure (p_1) and the operative inundation depth ($\alpha'\eta_{max}$) can be calculated based on the study conducted by Tanimoto et al. (1984), i.e., using η_{max} at the shoreline ($x = 0$), with $\alpha = 2.2$, and $\alpha' = 3$.

3.3 Overflow cases

3.3.1 Results

Figure 11 shows the laboratory images for the overflow cases, where t is the time after the tsunami generation (laboratory scale). After the tip of the tsunami flow reached the front of the seawall, the flow rose significantly and subsequently splashed down behind the seawall. The tsunami-induced force, defined as the difference in the vertically integrated wave pressures between the front and rear of the seawall, became maximum after the water level increased (**Figure 11(b)**, $t = 29.2$ s panel).
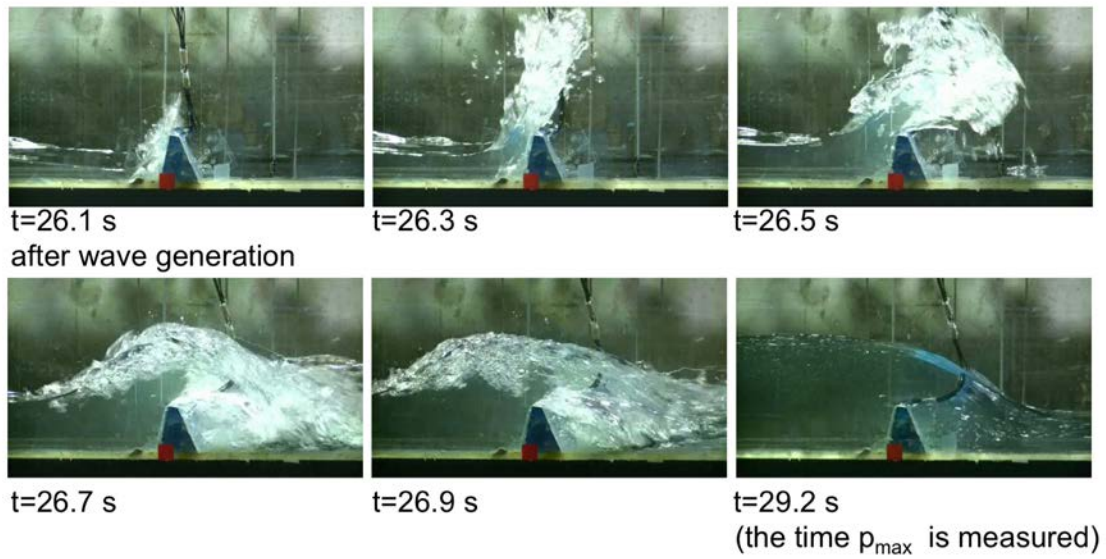
Figure 11: Laboratory images of overflow tsunami action (t indicates the time after wave generation).

Figure 12 compares the vertical profiles of $p_{max}/\rho g\eta$ on the shoreward side of the seawall, classified in terms of the slope of the bottom topography (s_B), distance from the shoreline (x), and the slope of the shoreward seawall (s_W), with those predicted by the hydrostatic pressure relation ($p_{max} = \alpha \times \rho g\eta$ with α = 1.0, 1.1, and 1.2). We found that $p_{max}/\rho g\eta$ was not considerably affected by the changes in the parameters, and the ratio of $p_{max}/\rho g\eta$ to the hydrostatic pressure was in the range of 1.0–1.2.

Figure 13(a) shows a scatterplot of h_c/η with respect to the correction factor (α_{E2}), defined in a manner similar to α_{E1} (4) as follows.

$$\alpha_{E2} = 1 + \overline{\frac{p_{max}}{\rho g\eta} - \left(1 - \frac{z}{\eta}\right)} \qquad (9)$$

where the overbar denotes the arithmetic mean of the data at the three points on the shoreward slope (**Figure 3(c)**). As the magnitude of the overflow decreases (i.e., as h_c/η approached 1), α_{E2} approaches a value in the range of 1.0–1.1. This agreed with the results obtained under the non-overflow cases ((7), **Figure 7**).

However, it should be noted that the numerical simulation of tsunami inundation used for the facility design (in Japan) sometimes cannot efficiently reproduce the water-level variation just in front of the seawall, because of its coarse spatial resolution (e.g., 5 m). Hence, we examined the relationship between the inundation depth ~ 20 m shoreward of the seawall (η_0) (see **Figure 3(c)**) and the shoreward wave pressure. **Figure 13(b)** shows a scatterplot of h_c/η_0 with respect to the correction factor (α_{E3}) defined using η_0 in a manner similar to (9). In this case, the correction factor was ~1.1 at maximum, which agreed with the results obtained under the non-overflow cases. From the scatterplot of the magnitude of overflow (h_c/η) with respect to the ratio η_0/η (**Figure 13(c)**), the two water levels tended to be largely the same (i.e., $\eta_0 \sim \eta$), as h_c/η approaches 1 but significantly different ($\eta_0 > \eta$) when $h_c/\eta < 1$, which is consistent with the difference between **Figures 13(a)** and **(b)**.

Finally, we examined the relationship between the landward wave pressure and the water level just behind the seawall (η_2, **Figure 3(c)**). Taking into account the possibility that the tsunami simulation used for the facility design cannot efficiently reproduce the corresponding water-level variation, the value of η_2 is determined from η using the Homma's formula, which was originally proposed for low overflow condition ($\eta_2 = 0.45h_1 + h_C$; see **Figure 3(c)**) (Homma 1940). **Figure 14(a)** shows a scatterplot of h_c/η_2 with respect to the correction factor (α_{E4}) (α_{E4} is defined in a manner similar to (9) using η_2). The correction factor for the landward wave pressure exceeded 0.4 for the high overflow cases ($h_c/\eta_2 < 0.8$), whereas it approached 0 for the low overflow cases ($0.8 < h_c/\eta_2 < 1$).

9
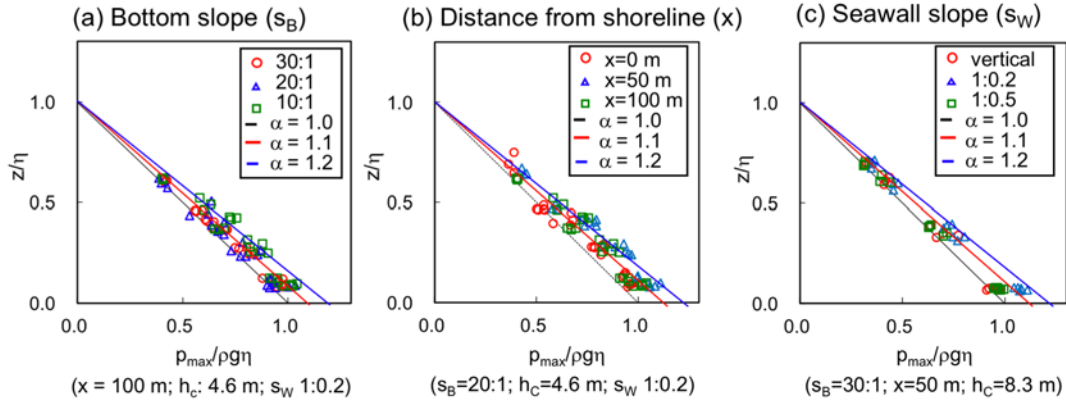
Figure 12: Comparison of vertical profiles of the shoreward $p_{max}/\rho g \eta$ classified in terms of (a) bottom slope, (b) distance from the shoreline, and (c) seawall slope; and those of the corresponding hydrostatic pressure ($p_{max} = \alpha \times \rho g \eta$). The blue, red, and black lines represent $\alpha = 1.2$, $\alpha = 1.1$ and $\alpha = 1.0$, respectively.
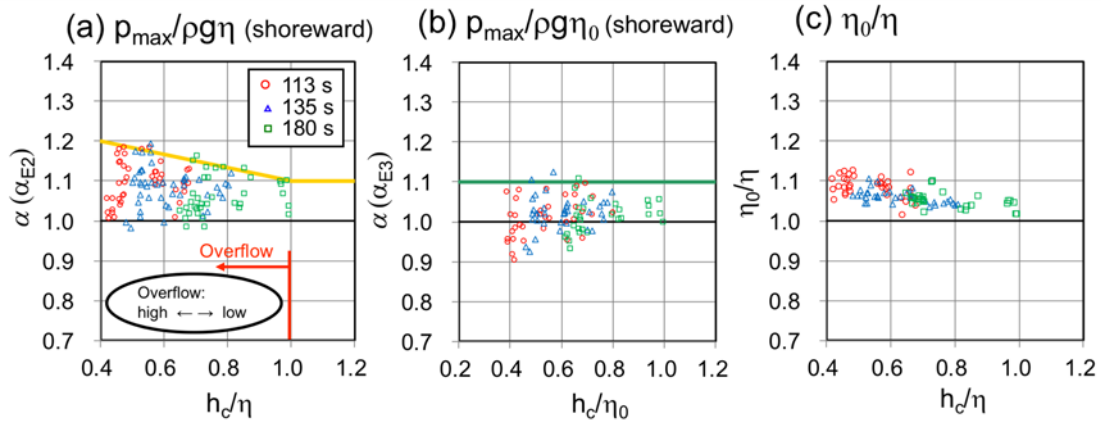
Figure 13: Scatterplots of (a) h_c/η versus α_{E2}, (b) h_c/η_0 versus α_{E3}, and (c) h_c/η versus η_0/η for shoreward slope.

Because the estimation of η_2 likely includes an uncertainty, particularly under high overflow conditions, we examined the vertical profiles of $p_{max}/\rho g \eta_B$, where η_B is the water level at ~10 m landward of the seawall (**Figure 3(c)**). The value of $p_{max}/\rho g \eta_B$ tend to be greater than 0.4 times that calculated using the hydrostatic pressure relation (i.e., $p_{max}/\rho g \eta_B = 0.4 \times (\eta_B - z)$; yellow line in **Figure 14 (b)**) for the large wave pressure depths ($z/\eta_B < \sim 0.3$).

3.3.2 Proposed formula

On the basis of the results obtained, we proposed formulae to calculate the tsunami-induced forces under the overflow condition to be used in the facility design, as shown below.

For the shoreward side of the seawall, the wave pressure (p_1 and p_2 in **Figure 4(c)**) is calculated using the inundation heights just in front of or somewhat shoreward of the seawall ($\eta_X = \eta_0$ or η) and the correction factor (α_I) such that

$$p_1 = \alpha_I \times \rho g \eta_X, \quad p_2 = p_1 (\eta_X - h_C)/\eta_X. \tag{10}$$

The correction factor (α_I) is determined as follows.

$$\alpha_I = 1.1 \tag{11}$$

when η_0 is known (see green line in **Figure 13(b)**). Alternatively, it can be calculated as follows.

$$\alpha_I = -0.17 \times h_C/\eta + 1.27 \tag{12}$$

10
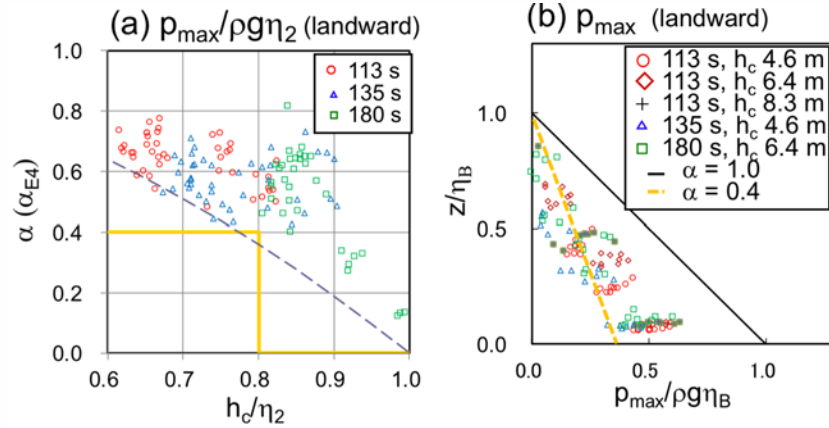
Figure 14: Scatterplots of (a) h_c/η_2 versus α_{E4}, and (b) $p_{max}/\rho g\eta_B$ versus z/η_B for landward slope.

when η is known (see yellow line in **Figure 13(a)**).

For the landward side of the seawall, the wave pressure (p_3 and p_4 in **Figure 4(c)**) is calculated using the inundation depths landward or just behind the seawall ($\eta_Y = \eta_B$ or η_2) and the correction factor (α_{IB}) such that

$$p_3 = \alpha_{IB} \times \rho g\eta_Y, \quad p_4 = p_1 \left(\eta_Y - h_{CB}^*\right)/\eta_Y, \quad h_{CB}^* = \min\left(h_C, \eta_Y\right). \qquad (13)$$

The correction factor (α_{IB}) is determined as follows.

$$\alpha_{IB} = 0.4 \quad \left(h_C/\eta_Y < 0.8\right)$$
$$\alpha_{IB} = 0 \quad\;\; \left(h_C/\eta_Y > 0.8\right) \qquad (14)$$

(see the yellow line in **Figure 14(a)**). The experiment results show that the correction factor (α_{E4}) decreases gradually as h_c/η_2 approaches unity (cf., dashed line in **Figure 14(a)**). However, although a detailed analysis is skipped, a numerical study reported that the value of α_{E4} fluctuated considerably and frequently approached 0 when $h_c/\eta_2 > 0.8$. Therefore, from a safety viewpoint, we consider that (14) is more appropriate at this point in time.

4. CONCLUSION

On the basis of the results of hydraulic model experiments, we explored the methods of calculating the tsunami-induced hydrodynamic forces under non-overflow and overflow conditions to be used in the facility design. Special attention was paid to modifications by incorporating a correction factor in the hydrostatic pressure relation.

Under the non-overflow condition, the tsunami-induced force acting on the seawall were appropriately evaluated using (1) the hydrostatic pressure relation and a correction factor of 1.1, and (2) a quadratic function of the Froude number (Fr). Furthermore, under the overflow condition, the forces were appropriately evaluated using the function of the inundation depths in front of and behind the seawalls. **Figure 15** shows the proposed formulae and a related flow diagram.

The conventional design methods for calculating tsunami-induced forces (in Japan) seldom considered the effects of dynamic pressure, the behavior under overflow conditions, nor the wave forces acting on the landward side of the seawalls. The present findings (e.g., **Figure 15**) were mentioned in the tentative design guideline for onshore seawalls, published by the Fisheries Agency and the Ministry of Land, Infrastructure, Transport, and Tourism in Japan (November, 2015; see http://www.jfa.maff.go.jp/j/gyoko_gyozyo/g_hourei/pdf/20151214.pdf (in Japanese)). We hope that the results of this study will
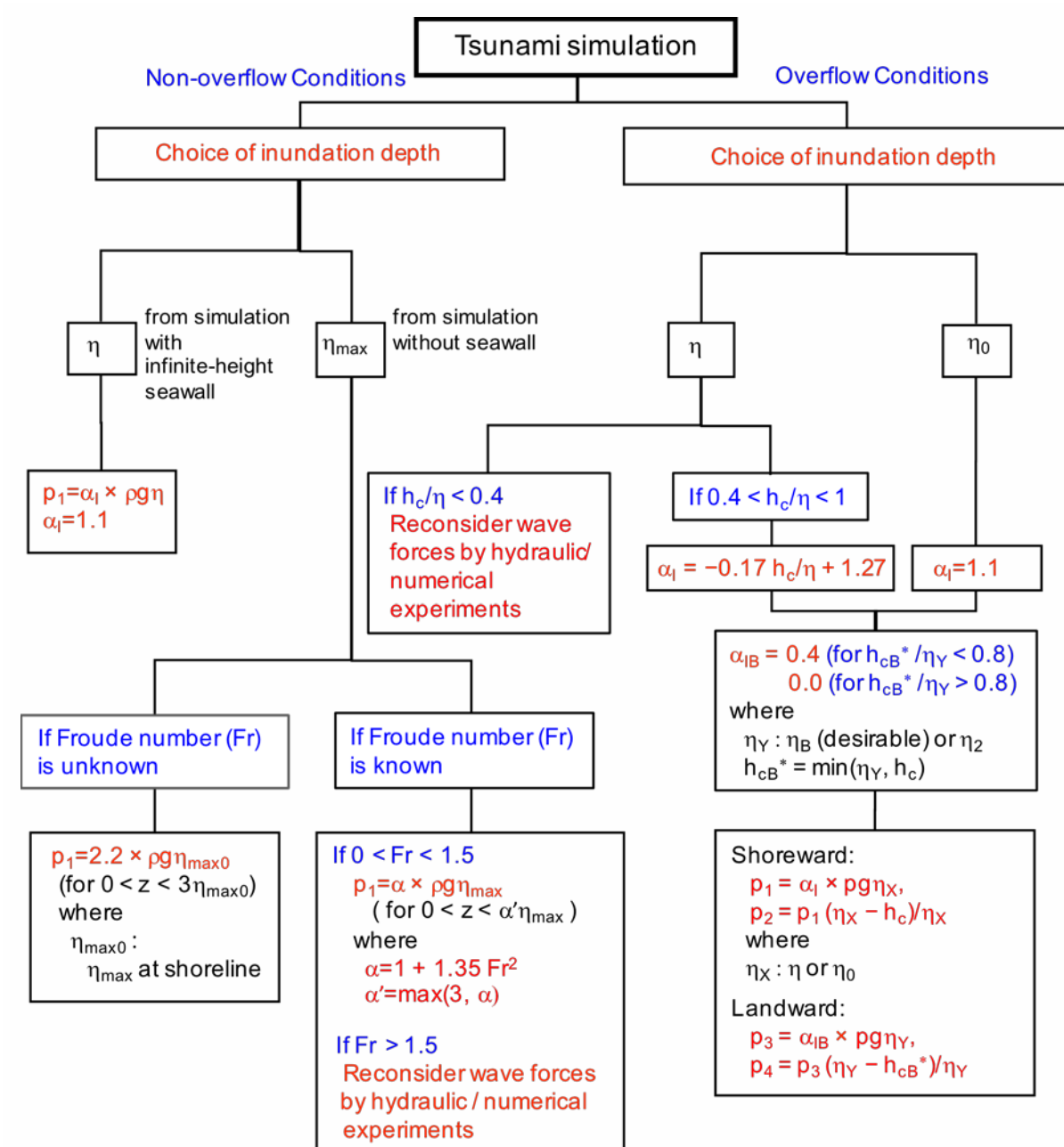
Figure 15: Flow diagram for calculating tsunami-induced forces. For definition of parameters, see Figures 3(c) and 4.

provide useful information in promoting disaster prevention and mitigation measures that will be effective against tsunamis.

Nevertheless, several issues need to be considered in future researches. First, the present study investigated the tsunami-induced forces acting on seawalls only in the horizontal direction. However, the vertical forces, such as the buoyancy force, might affect the stability of the structures. Furthermore, the present hydraulic experiment covered a limited range of parameters ($0.8 < Fr < 1.3$, and the ratio of the seawall height (h_c) to the inundation depth (i.e., η_0) was greater than 0.4; see **Figures 10 and 13**). Therefore, additional investigation is particularly required for tsunami cases when $Fr > 1.5$ or when $h_c < 0.4\eta_0$, if the corresponding wave pressure needs to be calculated (**Figure 15**) (in the present study, e.g., such a wave pressure might have been confirmed wherein the distance from the shoreline is greater than 150 m; see **Figure 5(c)**, or when $\eta_0 > 11.5$ m and/or $h_c < 4.6$ m). For the cases that surpass the design specification, studies on structural modifications, e.g., delaying the collapse due to tsunami are required. Further studies employing additional hydraulic experiments as well as numerical simulations at appropriate scales need to be conducted to address these issues.

Acknowledgments

References

Adriano, B., Hayashi, S., Gokon, H., Mas, E., Koshimura, S. (2016). Understanding the Extreme Tsunami Inundation in Onagawa Town by the 2011 Tohoku Earthquake, Its Effects in Urban Structures and Coastal Facilities, Coast. Eng. J., 58(4), 1640013, doi:10.1142/S0578563416400131.

Afmad, F., Shigihara, Y., Fujima, K., & Mizutani, N. (2009). A Study on Estimation of Tsunami Force Acting on Structures, J.JSCE (Ser.B2, Coastal Engineering), 65(1), 321-I_325 (in Japanese with an English abstract).

Asakura, R., Iwase, K., Ikeya, T., Takao, M., Kanto, T., Fujii, N., & Ohmori, M (2000). Experimental Study on Wave Force by Tsunami Overflowing Seawalls, Proc. Coastal Engineering, JSCE, 47, 911-915 (in Japanese with an English abstract).

Asakura, R., Iwase, K., Ikeya, T., Takao, M., Kanto, T., Fujii, N., & Ohmori, M (2002). The Tsunami Wave Force Acting on Land Structures, Proc. 28th ICCE, pp.1191-1202.

Homma, H. (1940). Coefficient of flow volume on low overflow weir., Civ. Eng. JSCE, 26 (6), 635-645 (in Japanese).

Japan Society of Civil Engineers (2004). Design Manual for Coastal Facilities 2000, 577 p. ISBN 4810604748.

Matsutomi, H., Kettoku, G., & Saitoh, M. (2013). Experiments on Tsunami Fluid Force Acting on a Reinforced Concrete Building with Aperture, J.JSCE (Ser.B2, Coastal Engineering), 69(2), 326-I_330 (in Japanese with an English abstract).

Nakamura, T., Sawa, Y., & Mizutani, N. (2016). Study of the Evaluation of Temporal Change in Horizontal and Vertical Tsunami Forces Acting on a Bridge Superstructure, Coast. Eng. J., 58(4), 1640020, doi:10.1142/S0578563416400209.

Ohmura, Y., Yagi, H., Nakayama, A., Mori, K., Kawano, D., Kato, H., Kado, A., & Namekawa, J. (2014). Experimental Study on Tsunami Induced Forces on Breast Type Seawalls Under Non-Overflow Condition, J.JSCE (Ser.B2, Coastal Engineering), 70(2), I_881-I_885 (in Japanese with an English abstract).

Ohmura, Y., Yagi, H., Nakayama, Yoneyama, M., Narita, T., Kato, H., Kado, A., & Namekawa, J. (2015). Experimental Study on Tsunami Induced Forces on Breast Type Seawalls, J.JSCE (Ser.B2, Coastal Engineering), 71(2), I_991-I_996 (in Japanese with an English abstract).

Sakakiyama, T (2012). Tsunami Inundation Flow and Tsunami Pressure on Structures, J.JSCE (Ser.B2, Coastal Engineering), 68(2), I_771-I_775 (in Japanese with an English abstract).

Tanimoto, K., Tsuruya, K., & Nakano, S. (1984). Study on Tsunami-Force and Disaster Cause of Landfill Seawall due to the tsunami by the 1983 Sea of Japan earthquake, Proc. Coastal Engineering, JSCE, 31, 257-261 (in Japanese).